Development and Experimental Validation of a Compressor Dynamic Model

M. Venturini
ENDIF - University of Ferrara,
Via Saragat, 1,
44100 Ferrara, Italy

In recent years, transient response analysis of energy systems is becoming more and more important in optimizing plant operation and control. Furthermore, dynamic analyses are also used to integrate steady-state diagnostic analyses, since they allow the detection of malfunctions characterized by time-dependent effects. The paper deals with the development of a nonlinear modular model for compressor dynamic simulation. After developing the compressor mathematical model through a physics-based approach (laws of conservation and thermal balances), the model is implemented through the MATLAB® SIMULINK® tool. Then, a sensitivity analysis is carried out to evaluate the influence of model parameters on the model response. Finally, the model is calibrated on a multistage axial-centrifugal small size compressor running in the test facility of the University of Ferrara (Italy) and validated through experimental data taken on the compressor under investigation. [DOI: 10.1115/1.1928935]

Introduction

The need for gas turbine simulation tools to carry out performance and diagnostic analyses is becoming ever greater. Thus, many studies have been carried out focusing on the development of useful tools able to support plant operation and/or to perform diagnostic analyses [1–4]. In particular, in addition to the analysis in steady-state conditions, there has been a growing interest in the dynamic behavior of energy systems, and so a great deal of research has also been aimed at developing dynamic simulation codes capable of reproducing transient system response [5–9].

In fact, the employment of simulation codes for transient behavior analysis finds useful application not only in power plants design phase and personnel training (as shown for instance in [9]) and in realizing plant control systems [10], but also proves particularly effective in investigating gas turbine component behavior under critical operating conditions [11] and in the presence of unsteady phenomena, such as stall and flutter [12–14], and of faults, especially those which can be recognized from unsteady data analysis [15,16]. In particular, in order to carry out diagnostic analyses, the availability of a dynamic simulation code allows:

- The identification of malfunctions which can be detected only during transient regimes (startup, acceleration, etc.) since they are characterized by time-dependent effects;
- The creation of a database of a great number of faults, together with the analysis of their effects on measurable variables (fault signature). Indeed, a series of experiments, intended to obtain such an amount of data, would be extremely expensive and difficult to perform;
- An automated diagnosis process to be performed through comparison between "healthy" and "faulty" component signatures in transient conditions, as a tool for supporting and integrating steady-state diagnostic analyses;
- The machine control system design in order to properly adapt the control logic to the actual health state of each component.

This paper deals with the development of a nonlinear modular model for the dynamic simulation of compressors. The model is implemented in MATLAB® environment through the SIMULINK® tool, which has proved to be a flexible and powerful tool for dynamic simulation [7,10,17].

The mathematical model is built in a general way through the laws of conservation (mass, momentum, energy, and moment of momentum) and heat balances, written in differential form, and by using the performance maps of the considered compressor, as done in [5,7,8,10,17]. The physics-based approach, since it requires knowledge of the phenomena taking place in the considered machine, allows a better understanding both of the physics of the processes and of the way each malfunction manifests itself, if compared to the use of "black box" models. On the other hand, the development of physics-based models presents some problems related to the quality of the calibration process. For this reason, a sensitivity analysis is carried out to evaluate the influence of the physical parameters, such as volume, friction factor, and heat transfer coefficient on model response.

Finally, the model is calibrated on a multistage axial-centrifugal small size compressor running in the test facility of the University of Ferrara (Italy) [18] and validated through experimental data taken on the compressor under investigation in different transient operating regimes.

Model Development

Mass, Momentum, and Energy Balance. The development of the physical-mathematical model to determine the laws of conservation (mass, momentum, and energy) is carried out starting from a general approach. For an infinitesimal control volume, let the frontal area be A and the infinitesimal thickness be dx. The balance for the *quantity* flowing per unit time through the control volume is

$$A\psi_e + Q_g dV = A\psi_l + \frac{\partial \Gamma}{\partial t} d\mathrm{V} \tag{1}$$

where ψ is the *quantity* flux, Γ the *quantity* concentration, Q_g the *quantity* generated per unit time and unit volume, and "e" and "l" the "entering" and "leaving" sections, respectively. It is worth noting that (i) the *quantity* has to be considered generated if it is generated inside the volume (as the mass generated in a nuclear reaction) and/or if its contribution is external to the system (as, for

Contributed by the International Gas Turbine Institute (IGTI) of THE AMERICAN SOCIETY OF MECHANICAL ENGINEERS for publication in the ASME JOURNAL OF TURBOMACHINERY. Paper presented at the International Gas Turbine and Aeroengine Congress and Exhibition, Vienna, Austria, June 13 – 17, 2004, Paper No. 2004-GT-53416. Manuscript received by IGTI, October 1, 2003; final revision, March 1, 2004. IGTI Review Chair: A. J. Strazisar.

example, the heat exchanged by the system with the outside), (ii) $\psi=\Gamma\nu$, where ν is the velocity of the fluid, and (iii) $dV=Adx$. By expressing function ψ through Taylor formula with Lagrange remainder, it is possible to obtain

$$\psi_l = \psi_e + \left.\frac{\partial\psi}{\partial x}\right|_{\xi} dx \quad \xi \in \,]0;\mathrm{dx}[$$

By substituting the above-derived expression for ψ_l into Eq. (1) and by dividing by dV, it is possible to obtain

$$\frac{\partial\psi}{\partial x} + \frac{\partial\Gamma}{\partial t} = Q_g \tag{2}$$

This general equation of conservation, obtained through the single hypothesis that the frontal area A is constant, allows the laws of conservation (mass, momentum, and energy) to be derived in a form similar as that reported in [8].

In the case of mass balance, the *quantity* is the mass, Γ is the density ρ, while $\psi=\rho\nu$. Since Q_g is equal to zero, the following equation can be obtained:

$$\frac{\partial\rho v}{\partial x} + \frac{\partial\rho}{\partial t} = 0 \tag{3}$$

In the case of momentum balance, the *quantity* is the momentum, Γ is the product $\rho\nu$, while $\psi=\rho\nu^2$. Q_g is equal to the sum of the external forces per unit volume acting on the system, i.e., pressure, friction, and body field forces. In this case, the momentum balance equation can be written as

$$\frac{\partial(\rho\nu^2)}{\partial x} + \frac{\partial\rho\nu}{\partial t} = \sum f = -\frac{\partial p}{\partial x} - f_{fr} - f_{bf}$$

By neglecting the body field forces (mainly due to gravitational field contribution) and by rearranging the terms, the following equation can be obtained:

$$\frac{\partial(p+\rho\nu^2)}{\partial x} + \frac{\partial\rho\nu}{\partial t} = -f_{fr} \tag{4}$$

In the case of energy balance, the *quantity* is the energy e, obtained as the sum of three contributions (internal energy u, body potential energy e_p, and kinetic energy), Γ is equal to ρe, while Q_g is equal to the sum of external heat and work per unit volume exchanged by the system with the outside. By isolating the term of pressure forces and by taking it to the left-hand side of the equation, the following general expression for energy balance can be obtained:

$$\frac{\partial}{\partial x}\left[\rho\nu\left(u + e_p + \frac{\nu^2}{2} + \frac{p}{\rho}\right)\right] + \frac{\partial}{\partial t}\left[\rho\left(u + e_p + \frac{\nu^2}{2}\right)\right] = q - l \tag{5}$$

Moment of Momentum Balance. The well-known equation for moment of momentum balance can be written as

$$J\frac{2\pi}{60}\frac{dN}{dt} = \mathrm{Tq}_s - \mathrm{Tq}_r - \mathrm{Tq}_{\mathrm{fr}} \tag{6}$$

where the three contributions on the right-hand side are due (i) to the torque Tq_s externally supplied (by a turbine or by a motor), (ii) to the resisting torque Tq_r, and (iii) to the torque $\mathrm{Tq}_{\mathrm{fr}}$ due to friction losses. The moment of inertia J is the total moment of inertia calculated with respect to the shaft for which the rotational speed N is evaluated.

Thermal Balance. In order to take into account the thermal phenomena which take place in the system under consideration, the Fourier flux law and the Fourier equation can be used.

The heat transfer from a surface to the free stream can be obtained by means of the balance of heat fluxes at the wall

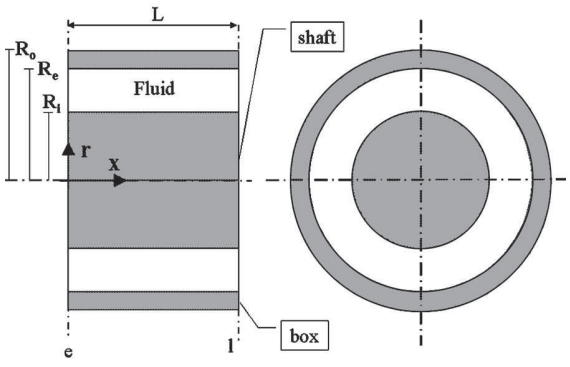

Fig. 1 Module geometrical model

$$\alpha(T_w - T) = -k\,\nabla T|_w \tag{7}$$

where T_w and T are the wall and free stream temperatures, respectively, and the term on the right-hand side is derived from the Fourier flux law at the wall. In Eq. (7), the surface is assumed to be at a higher temperature than the free stream.

If the term of energy generation is considered to be zero, the Fourier equation can be written as

$$\rho c\frac{\partial T}{\partial t} = k\nabla^2 T \tag{8}$$

Simplified Form of Balance Equations. Owing to the different gas turbine design characteristics (size, geometry, cooling devices, etc.) that can be encountered in practice, the first hypothesis which is introduced into the model deals with the geometry of the system. It is assumed that each component of a gas turbine can be modeled through one or more annular-shaped cylindrical modules whose length is L and whose internal and external radius are equal to R_i and R_e, respectively. As reported in Fig. 1, the fluid flows between an element called *shaft*, which plays the role of the component rotational shaft, and an element called *box*, representing the component external casing.

According to the model geometrical assumptions, a simplified expression for mass and momentum balance is derived under the following additional hypotheses, by integrating Eqs. (3) and (4) over volume Adx from the "entering" to "leaving" sections

1. Gas state equation $p/\rho=\mathrm{RT}$ and $c_p=c_p(T)$;
2. Constant gas properties in each x section;
3. Isentropic transformation (i.e., $p\rho^{-k}$=constant) and, so, by differentiating, $dp=kRTd\rho$;
4. Expression of friction forces as

$$f_{\mathrm{fr}} = \frac{\lambda}{D_h}\rho\frac{\mathrm{v}^2}{2}$$

Moreover, as shown in [5,7,8], for short-length pipes it is acceptable to integrate along x only the terms in the x derivatives, while, in the other terms (t derivatives and friction forces), T, p, and M can be considered constant with respect to x. In particular, the constant-with-x values for T and M have been assumed equal to their value in the "leaving" section, while p has been assumed equal to the value in the "entering" section in Eq. (9) and equal to the mean value between the two sections in Eq. (10), i.e., $(p_e+p_1)/2$. Thus the new expression of Eqs. (3) and (4) is

$$\frac{\partial p_e}{\partial t} = \frac{k\mathrm{RT}_1}{AL}(M_e - M_l) \tag{9}$$

$$\begin{cases} \dfrac{\partial M_l}{\partial t} = \dfrac{A}{L}(p_e - p_l) - \dfrac{\lambda}{D_h}\dfrac{R}{A}\dfrac{M_l^2 T_l}{(p_e + p_l)} - o \\ o = \dfrac{R}{\mathrm{AL}}\left(M_l^2 \dfrac{T_l}{p_l} - M_e^2 \dfrac{T_e}{p_e}\right) \end{cases} \tag{10}$$

In the general case of long-length pipes, the integration along x can be performed by representing each component as the sum of a series of short-length pipes.

A simplified expression for thermal balance equations was also derived. For the *box* element Eq. (7), written at $r=R_e$ and $r=R_o$, leads to

$$\alpha_e(T - T_{be}) = -k_b[\nabla T_b]_{r=R_e} \tag{11}$$

$$\alpha_o(T_{\mathrm{bo}} - T_{\infty b}) = -k_b[\nabla T_b]_{r=R_o} \tag{12}$$

where the negative sign on the right-hand side of the equations is in accordance with the choice of r versus and $T_{\infty b}$ is the temperature of the environment outside the compressor casing, generally equal to ambient temperature. Temperatures T_{be} and T_{bo} are *box* wall temperatures at $r=R_e$ and $r=R_o$, respectively. From Eq. (8) for the *box* element, it is then possible to obtain

$$\rho_b c_b \frac{\partial T_b}{\partial t} = k_b \nabla^2 T_b \tag{13}$$

By writing Eqs. (11), (12), and (13) in cylindrical coordinates and by assuming that (i) heat fluxes $\alpha_e(T-T_{\mathrm{be}})$ and $\alpha_o(T_{\mathrm{bo}}-T_{\infty b})$ have radial direction and (ii) T_b does not depend on x coordinate, it is possible to obtain

$$\alpha_e A_e(T - T_{\mathrm{be}}) = -k_b A_e \left[\frac{\partial T_b}{\partial r}\right]_{r=R_e} \tag{14}$$

$$\alpha_o A_o(T_{\mathrm{bo}} - T_{\infty b}) = -k_b A_o \left[\frac{\partial T_b}{\partial r}\right]_{r=R_o} \tag{15}$$

$$\rho_b c_b \frac{\partial T_b}{\partial t} = \frac{k_b}{r}\frac{\partial}{\partial r}\left(r\frac{\partial T_b}{\partial r}\right) \tag{16}$$

By integrating Eq. (16) between R_{e} and R_{o}, the following expression can be derived:

$$\int_{R_e}^{R_o} \rho_b c_b \frac{\partial T_b}{\partial t} r dr = k_b \left[r\frac{\partial T_b}{\partial r}\right]_{R_e}^{R_o} \tag{17}$$

If it is supposed that T_b does not depend on coordinate r (i.e., $T_{\mathrm{be}}=T_{\mathrm{bo}}=T_{\mathrm{b}}$) and Eqs. (14) and (15) are substituted into Eq. (17), it is possible to obtain

$$\rho_b c_b V_b \frac{\partial T_b}{\partial t} = \alpha_e A_e(T - T_b) - \alpha_o A_o(T_b - T_{\infty b}) \tag{18}$$

where $A_e=2\pi R_e L$, $A_o=2\pi R_o L$ and $V_b=\pi(R_o^2-R_e^2)L$. This equation was derived under the hypothesis that T_b does not depend on coordinates r and x, which, in turn, means that fluid conductivity is negligible if compared to *box* conductivity.

In a similar way, the thermal balance equation for the *shaft* element can be obtained

$$\rho_s c_s V_s \frac{\partial T_s}{\partial t} = \alpha_i A_i(T - T_s) - \alpha_{\mathrm{cool}} A_i(T_s - T_{\infty s}) \tag{19}$$

In particular, the term $\alpha_{\mathrm{cool}}A_i(T_s-T_{\infty s})$ accounts for the heat flow in steady-state conditions (the shaft does not have the same temperature as the gas flow in steady-state conditions, since it is not isolated from external environment), while $T_{\infty s}$ is the *shaft* cooling temperature, which can be assumed equal to the ambient or to the lube-oil temperature.

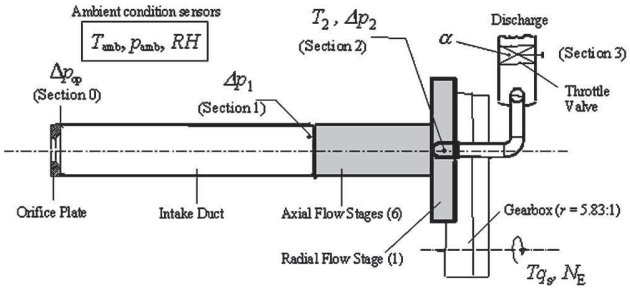

Fig. 2 Compressor test rig and measured variables

Compressor Under Investigation

Test Rig. The test facility under consideration, described in detail in [18], consists of an asynchronous reversible electric motor/brake bench, operated by an inverter. The motor can give a maximum power of 87 kW at 5000 rpm.

Compressor. The compressor, which is part of the Allison 250-C18 turbo-shaft engine, is composed of six axial stages and one centrifugal stage. The compressor operates in an open circuit. As schematically sketched in Fig. 2, the inlet section (an orifice plate) is followed by a pipe, used to perform the inlet mass flow measurement. Then, after flowing through the axial and centrifugal stages, the air is fed to a discharge volume in which a butterfly valve, whose angular position is indicated by α, is inserted for compressor mass flow rate control. A step-up gearbox with a gear ratio r equal to 5.83 (which was part of the original gas turbine) is included in the test setup to analyze a range of compressor rotational speeds up to nearly 30, 000 rpm.

Measurable Variables. Among all the available measurable variables taken on the compressor, the available measurements used for model development and validation are indicated in Fig. 2:

- Ambient temperature, pressure, and relative humidity (T_{amb}, p_{amb}, and RH), which define ambient conditions both at the inlet and at the outlet of the test facility ($T_0=T_{\mathrm{amb}}$ and $p_3=p_{\mathrm{amb}}$);
- Static differential pressure measurements Δp_{op}, Δp_1, and Δp_2. The differential pressure measurement at the orifice plate Δp_{op} is carried out in order to perform the inlet mass flow measurement, while Δp_1 and Δp_2 allow the determination of compressor pressure ratio β_{C};
- Total outlet compressor temperature T_2;
- Rotational speed of the electric motor shaft N_E and shaft torque $\mathrm{Tq_s}$. These measurements allow the determination of the power required to drive the compressor.

Performance Maps. The evaluation of compressor performance maps was carried out in steady-state conditions [18], thus allowing the polytropic efficiency η_C and the pressure ratio β_C to be expressed against the corrected mass flow μ_C for different values of the corrected rotational speed ν_C. In particular, the rotational speed of the compressor can be calculated from the shaft rotational speed by means of the relationship $N_C=rN_E$. The maps, reported in Figs. 3(a) and 3(b), were determined experimentally for different compressor rotational speeds (in the range 6000–30,000 rpm) and were then interpolated by means of a second degree polynomial curve.

Moreover, the region of compressor normal operation was identified between the surge line (occurrence of unsteady phenomena such as surge and/or rotating stall, which were detected by analyzing the dynamic trends of discharge pressure and suction mass flow rate [18]) and the line interpolating the operating points for which the throttle valve was fully open.

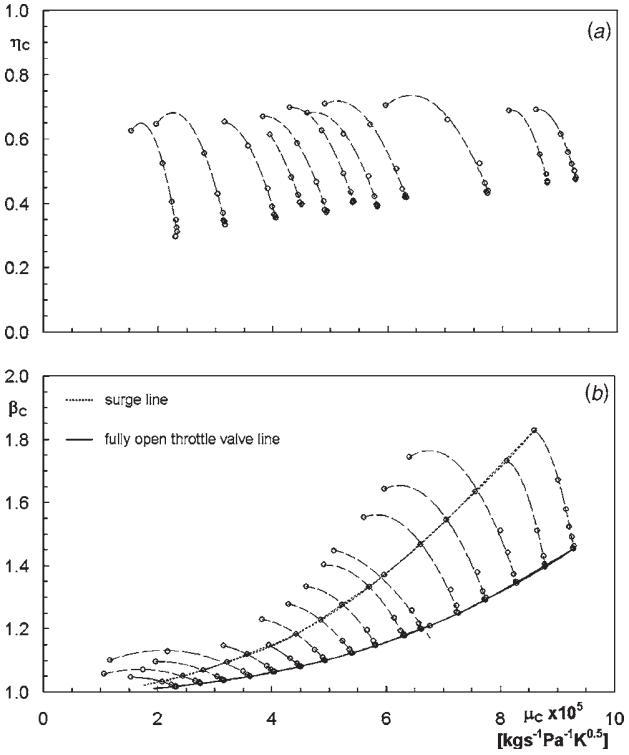

Fig. 3 Compressor performance maps: (◯) measured value; (---) second degree polynomial interpolating curve

Model Implementation

The model is implemented in MATLAB® environment through the SIMULINK® tool, which allows dynamic systems to be modeled through a user-friendly graphical interface. SIMULINK® proved particularly effective since it offered the possibility (i) to create new functions in addition to the libraries which are already available and (ii) to perform the solution of equations through different solvers. In particular, for all the developed modules, a variable-step integration algorithm was used.

A modular structure for system modeling was adopted, by identifying three subsystems (*intake duct, compressor*, and *exhaust duct*), which are sketched in Fig. 4 and are described in detail in the following sections. Each component is modeled by means of a single module, by assuming that the simplification for short-length pipes is acceptable, as previously discussed.

In particular, the *compressor* module is formed by the sum of two submodules, one for "static" and one for "dynamic" simulation [5]. In fact, rises in pressure and temperature in steady-state

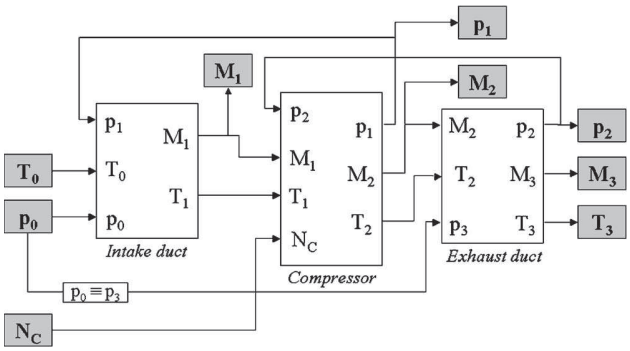

Fig. 4 Model implementation through the SIMULINK® tool

conditions along the compressor are taken into account by means of machine performance maps, while balance equations are used in order to consider mass storage and thermal exchange phenomena.

Mass storage effects in the suction and discharge piping systems are taken into account through the *intake* and *exhaust duct* modules. In particular, the application of Eq. (10) to these two modules has shown that the term o in Eq. (10) is negligible and, thus, it has been neglected. The reason for this can be attributed to the fact that the considered test facility is characterized by relatively short length piping volumes and, as a result, storage effects are not very significant. In fact, this implies that $M_e \approx M_1$ and $p_e \approx p_l$, which, in addition to the assumption that $T_e = T_l$ for both modules, finally leads to the conclusion that o is indeed negligible.

Intake Duct Module. The *intake duct* module inputs are ambient pressure p_0 and temperature T_0 and pressure p_1 (from *compressor* module). In order to calculate module outputs, the following equations are used:

- T_1 is assumed equal to T_0, by considering negligible the thermal exchange in the *intake duct*;
- M_1 is determined by means of Eq. (20), which derives from Eq. (10) calculated between sections "0" and "1", and by ignoring the term o on the right-hand side, as anticipated. Thus, the final form of the equation is the following:

$$\frac{\partial M_1}{\partial t} = \frac{A}{L}(p_0 - p_1) - \frac{\lambda}{D_h}\frac{R}{A}\frac{M_1^2 T_1}{(p_0 + p_1)} \tag{20}$$

Compressor Module. The *compressor* module requires the information derived from performance maps and takes into account the presence of heat transfer phenomena.

The *compressor* module inputs are compressor rotational speed N_C, M_1, and T_1 (from *intake duct* module) and pressure p_2 (from *exhaust duct* module). Three outputs are calculated from the module: entering pressure p_1, leaving mass flow rate M_2, and temperature T_2.

Entering pressure p_1 is determined by means of Eq. (21), which derives from Eq. (9) calculated between sections "1" and "2"

$$\frac{\partial p_1}{\partial t} = \frac{kRT_1}{AL}(M_1 - M_2) \tag{21}$$

Since p_2 is an input and p_1 is determined from Eq. (21), compressor pressure ratio is known and, thus, leaving mass flow rate M_2 can be determined from compressor performance map reported in Fig. 3(b). Once the leaving mass flow rate M_2 is known, compressor polytropic efficiency can be determined from the compressor efficiency performance map [Fig. 3(a)]. To do this, *ad hoc* libraries were developed in order to interpolate the curves and to determine the current M_2 value. In particular, a control is performed to verify whether the compressor is working in the region between the surge line and the fully open throttle valve line.

From knowledge of compressor polytropic efficiency, it is possible to calculate the "stationary" (i.e., without taking into account thermal exchange phenomena in unsteady conditions) compressor leaving temperature $T_{2\text{stat}}$ as

$$T_{2\text{stat}} = T_1\left(\frac{p_2}{p_1}\right)^{(k-1)/(k\eta_c)}$$

Finally, the compressor leaving temperature T_2 is determined by solving the equation below

$$T_2 = T_{2\text{stat}} - \frac{1}{M_2 c_p}\left(\rho_s c_s V_s \frac{\partial T_s}{\partial t} + \rho_b c_b V_b \frac{\partial T_b}{\partial t}\right) \tag{22}$$

where temperature derivatives can be determined by means of Eqs. (18) and (19).

Table 1 Geometrical parameters (D_h and L) and friction factors (λ) used for model calibration estimated parameters indicated in boldface

	D_h[m]	L[m]	λ
Intake duct	0.1	1.00	**0.20**
Compressor	0.1	0.40	
Exhaust duct	**0.1**	**0.79**	**2.05**

Table 2 Heat transfer parameters

Quantity	Value	Quantity	Value
A_i	0.0653 m^2	α_i	100.0 W/(m^2 K)
A_e	0.1260 m^2	α_e	100.0 W/(m^2 K)
A_o	0.1280 m^2	α_o	10.0 W/(m^2 K)
C_s	159 J/K	$\alpha_{cool}A_i$	0.3 W/K
C_b	315 J/K	T_{oil}	285 K

Exhaust Duct Module. The *exhaust duct* module inputs are pressure p_3 (equal to ambient pressure p_0), temperature T_2, and mass flow rate M_2 (these two latter from *compressor* module). In order to calculate module outputs (T_3, p_2, and M_3), the following equations were used:

- T_3 is assumed equal to T_2, by considering negligible the thermal exchange in the *exhaust duct*;
- Entering pressure p_2 is determined by means of Eq. (23), which derives from Eq. (9) calculated between sections "2" and "3"

$$\frac{\partial p_2}{\partial t} = \frac{kRT_2}{AL}(M_2 - M_3) \tag{23}$$

- M_3 is determined by means of Eq. (24), which derives from Eq. (10) calculated between sections "2" and "3," and by ignoring the term o on the right-hand side. Thus, the final form of the equation is the following:

$$\frac{\partial M_3}{\partial t} = \frac{A}{L}(p_2 - p_3) - \frac{\lambda}{D_h}\frac{R}{A}\frac{M_3^2 T_3}{(p_2 + p_3)} \tag{24}$$

Model Calibration

Geometrical Parameters and Friction Factors. The geometrical parameters (D_h and L) and the friction factors (λ) which were used to set up the model on the compressor under investigation are reported in Table 1 for the three modules.

According to model assumptions, the compressor geometry was assumed cylindrical, with mean hydraulic diameter equal to 0.1 m and length L equal to 0.4 m.

The determination of the intake duct friction factor λ was performed by using Eq. (20) in steady-state conditions which assumes the form of Eq. (25) in which λ is the only unknown.

$$\frac{A}{L}(p_0 - p_1) = \frac{\lambda}{D_h}\frac{R}{A}\frac{M_1^2 T_1}{(p_0 + p_1)} \tag{25}$$

As regards compressor discharge, whose geometry is quite complex (two pipes which converge into a common discharge volume), the unknowns are three (D_h, L, and λ) and, so, a system of three equations was considered. The procedure for the calculation of the unknowns is as follows:

- Equation (24) is written for three different transient conditions corresponding to the same measured inlet mass flow rate. In fact, if steady-state data were used, the three equations would not be independent from each other;
- It was assumed $M_3 \approx M_0$ (M_0 is a measured quantity) and the derivative $\partial M_3/\partial t$ was evaluated numerically;
- The equation system was solved approximately, by introducing into each equation of the system the bias σ

$$\frac{\partial M_3}{\partial t} - \frac{A}{L}(p_2 - p_3) + \frac{\lambda}{D_h}\frac{R}{A}\frac{M_3^2 T_3}{(p_2 + p_3)} + \sigma = 0 \tag{26}$$

- The values of D_h, L, and λ which minimized the sum of the absolute values of the bias σ in the three equations were adopted for model calibration.

The numerical results of the procedure applied to the exhaust duct are reported in the third row of Table 1.

Heat Transfer. The quantities associated with the presence of heat transfer (exchange areas, heat transfer coefficients, and thermal capacities) were estimated according to the following assumptions:

- Shaft and box elements are realized in aluminum (ρ=2700 kg/m^3; c=921 J/(kg K); k=210 W/(m K));
- Heat transfer mechanism from box to outside: natural convection;
- Heat transfer mechanism from fluid to box and from fluid to shaft: forced convection.

The heat transfer parameter values adopted in the model are reported in detail in Table 2.

Model Sensitivity Analysis

The influence of geometrical parameters and of friction factors on the model output response (p_1, p_2, M_1, and T_2) was evaluated. A variation of ±10% for each parameter was considered for different values of the rotational speed and the relative variation ΔQ of each output Q was evaluated as

$$\Delta Q = \frac{Q - Q_{ref}}{Q_{ref}}$$

where Q_{ref} is the Q value in correspondence to the reference value of the considered parameter (reported in Tables 1 and 2).

The most interesting results are presented in the following sections for the friction factors of intake duct λ_{1-2} and exhaust duct λ_{2-3} and for exhaust duct hydraulic mean diameter $(D_h)_{2-3}$ and length L_{2-3} in the case of compressor rotational speed N_C equal to 29,150 rpm. The results for heat transfer coefficients are not reported in the paper since it was observed that the influence on all outputs was negligible, since they only affect model transient response, as can be seen from Eq. (22).

Intake Duct Friction Factor. It can be observed (Fig. 5) that

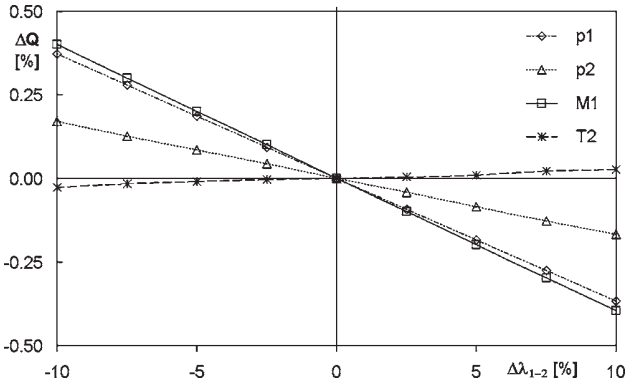

Fig. 5 Intake duct friction factor influence

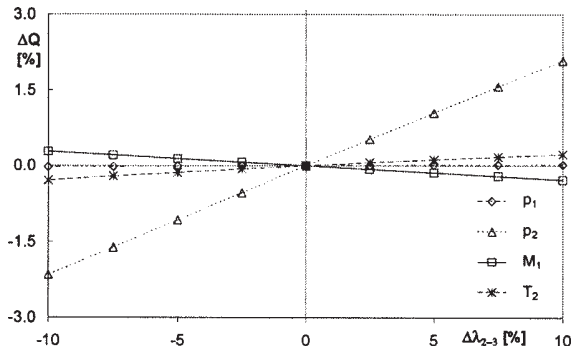

Fig. 6 Exhaust duct friction factor influence

(i) the dependence of all quantities is linear and (ii) p_1 and M_1 are the most sensitive to this parameter, while the influence on T_2 is negligible. In any case, the influence of this parameter on model output is very small: In fact, the order of magnitude of output sensitivity is of about 0.5% with respect to a 10% friction factor variation.

Exhaust Duct Friction Factor. It can be observed (Fig. 6) that (i) the dependence of all quantities is linear, (ii) p_2 is the most sensitive (up to 2%), while p_1 remains almost constant. This implies that the pressure ratio increases and, so, according to the performance maps, the mass flow rate M_1 slightly decreases, while the influence on T_2 is still negligible, according to the fact that the compressor efficiency increases. Furthermore, the evaluation of the influence of exhaust duct length on model response showed that the results are exactly the same as those obtained for exhaust duct friction factor influence, according to Eq. (24).

Exhaust Duct Hydraulic Mean Diameter. As shown in the previous section (Table 1), such a parameter could not be measured and, so, it was estimated. For this reason, the sensitivity analysis proves to be particularly helpful in order to correctly tune the model. In particular, it can be observed from Fig. 7 that an increase in the exhaust duct hydraulic mean diameter allows a greater mass flow rate (up to +1%), though the trend shows a "saturation" effect. Such behavior can be attributed to the fact that, though $(D_h)_{2-3}$ increases and, as a result, the discharge flow-through area increases, the inlet flow-through area remains the same. Moreover, p_1 remains constant, while p_2 decreases significantly (−7.5%), according to the trend of the compressor performance maps. The strong decrease of compressor pressure ratio also leads to a decrease in temperature T_2(−1.5%).

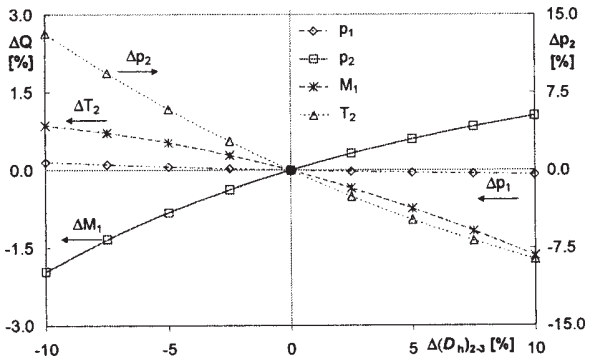

Fig. 7 Exhaust duct hydraulic mean diameter influence

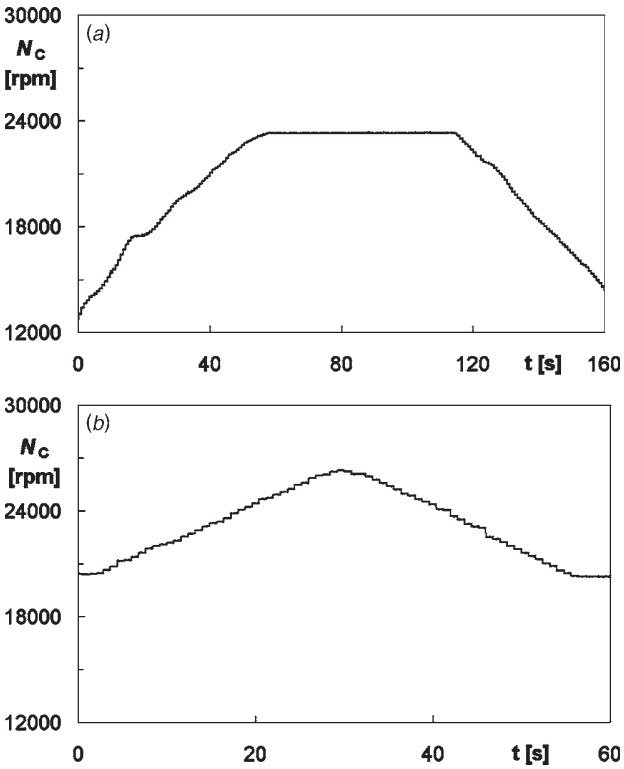

Fig. 8 Rotational speed profile versus time for the two test cases (*a*) *TC*1; (*b*) *TC*2

Model Validation

The developed model was validated by comparing the program response for all outputs (p_1, p_2, M_1, and T_2) against the corresponding measured values: This was possible for pressures p_1 and p_2 and temperature T_2 (the values of these quantities are both measured and computed by the program), while the mass flow rate M_1 was compared with the M_0 measured value since the measurement of M_1 is not available. This latter assumption is valid only in steady-state conditions, i.e., if mass storage effect is negligible between sections "0" and "1," and can be also considered acceptable in unsteady conditions due to *intake duct* small volume.

Two test cases were considered (*TC*1 and *TC*2, whose rotational speed trend is reported in Fig. 8), both taken at quasi-imaginary spin orbit (ISO) conditions ($T_{amb} \approx 17°C$; $p_{amb} \approx 102$ kPa) and representing acceleration and deceleration maneuvers for the compressor. The curves differ from each other since the *TC*1 curve covers a wide range of variation for compressor rotational speed (N_C ranges from about 13,000 up to 23,000 rpm), though rather slowly (160 s), while the *TC*2 curve is more rapid (acceleration in about 30 s), though in a more restricted region of N_C values (from about 20,000 up to 26,000 rpm).

The results of the comparison between measured and predicted values are presented in Figs. 9 and 10. For both test cases, it can be observed that predicted values are generally in good agreement with measured values, since (i) the shape of the predicted curve closely follows the experimental data and (ii) model inertia seems to be the same as physical system inertia (i.e., there is no appreciable delay between model and system response). In particular:

- p_1 is overestimated for low values of the rotational speed (Figs. 9(*a*) and 10(*a*));
- p_2 is underestimated for high values of the rotational speed, mainly in the case of the *TC*2 curve (Fig. 10(*b*));
- The error in predicting the mass flow rate is more evident in

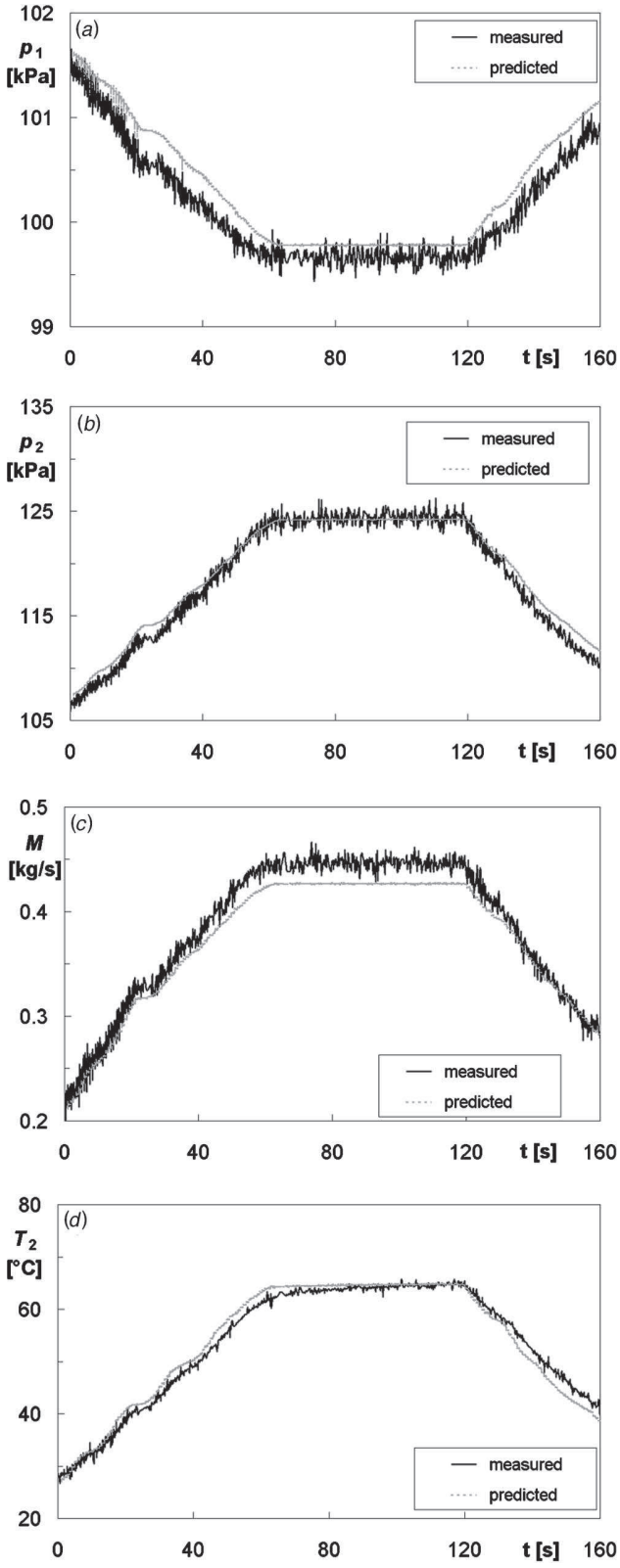

Fig. 9 Comparison of predictions and measured values for the *TC*1 curve: inlet (*a*) and outlet (*b*) compressor pressure, mass flow rate (*c*), and outlet compressor temperature (*d*)

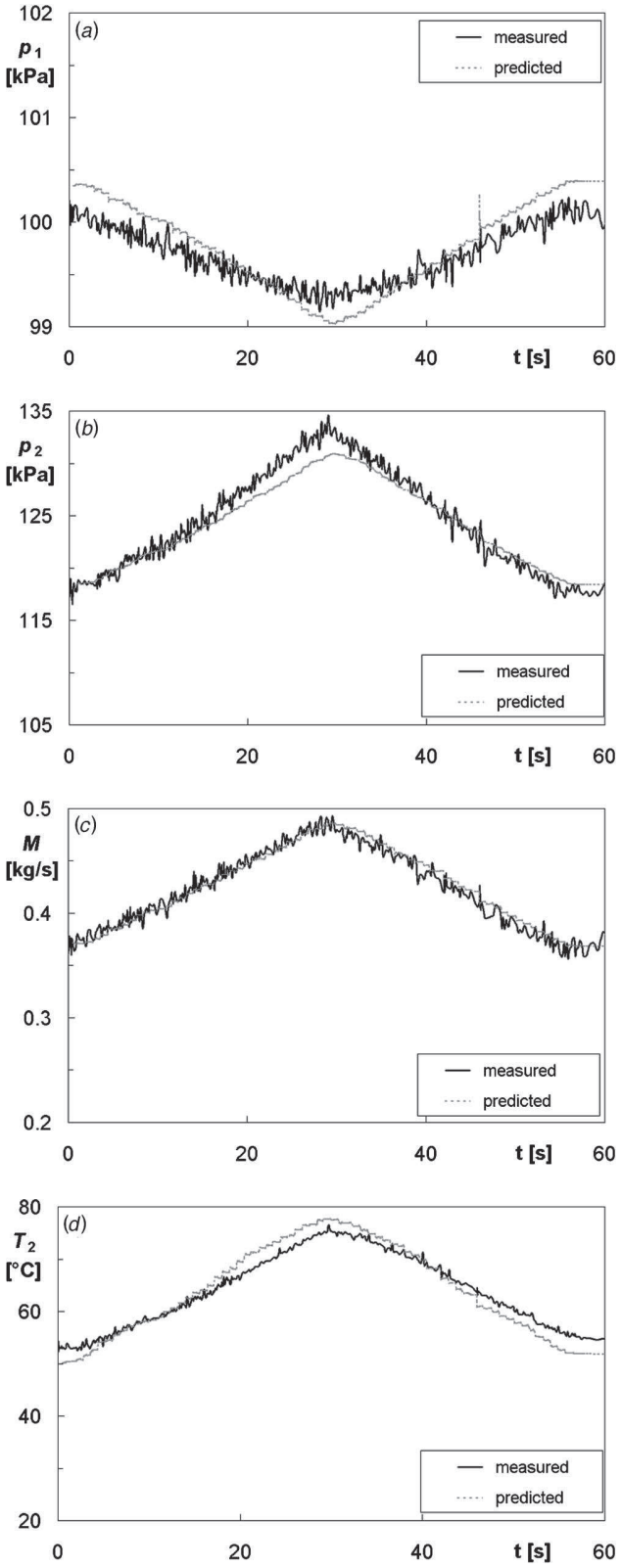

Fig. 10 Comparison of predictions and measured values for the *TC*2 curve: inlet (*a*) and outlet (*b*) compressor pressure, mass flow rate (*c*), and outlet compressor temperature (*d*)

Table 3 Maximum absolute value and standard deviation of errors and RMSE values between computed and predicted values

	TC1	*TC2*	*TC1*	*TC2*	*TC1*	*TC2*
Quantity	Max error	Max error	Stand. Dev.	Stand. Dev.	RMSE [%]	RMSE [%]
p_1[kPa]	0.531	0.481	0.234	0.207	0.233	0.207
p_2[kPa]	2.294	3.925	0.902	1.216	0.794	0.945
M_0[kg/s]	0.040	0.020	0.015	0.007	3.963	1.692
T_2[°C]	4.305	4.431	1.512	2.008	0.472	0.595
Overall					2.038	1.019

the steady-state phase of the *TC*1 curve (Fig. 9(*c*)), while in the *TC*2 curve, which is characterized only by transient regime, this effect is not detectable (Fig. 10(*c*)). This suggests the need for better tuning of the model in reproducing compressor steady-state behavior;

- T_2 is reproduced accurately in the *TC*1 curve, while in the *TC*2 curve the accordance is less evident, though the absolute error between measured and predicted values is small (about 2 °C).

In Table 3, the maximum absolute value and standard deviation of errors between computed and predicted values are reported. For the calculation of maximum absolute value and standard deviation of errors only measured and predicted values after 1 s from the beginning of the maneuvers were considered: This was done since simulated values at the beginning of the simulation are heavily influenced by model initial condition and, so, model prediction error was extremely high.

The analysis of the results presented in Table 3 shows that maximum absolute errors are very small for inlet compressor pressure p_1 (maximum value of about 0.5 kPa), while errors are more significant for outlet compressor pressure p_2 (up to 4.0 kPa) though errors are more uniformly distributed (i.e., the ratio between the standard deviation and the maximum absolute value is lower). Absolute errors between predicted and measured values also seem significant for the mass flow rate (up to 0.04 kg/s) in particular for *TC*1, if compared with measured values (highest measured mass flow rate equal to 0.45 kg/s). The greatest difference between computed and measured values of the outlet compressor temperature T_2 is of about 4.4 °C.

Moreover, Table 3 also shows the values of the root mean square error (RMSE), expressed in percentage, made by the model on the whole set of measured data for each output (p_1, p_2, M_1, and T_2) and for each curve, according to formula (27)

$$\mathrm{RMSE} = \sqrt{\frac{1}{n_{\mathrm{pred}}}\sum_{i=1}^{n_{\mathrm{pred}}}\left(\frac{Q_{\mathrm{meas},i} - Q_{\mathrm{pred},i}}{Q_{\mathrm{meas},i}}\right)^2} \tag{27}$$

where $Q_{\mathrm{meas},i}$ are the measured values, $Q_{\mathrm{pred},i}$ the values predicted through the model and n_{pred} is the number of predicted values (equal to 1383 or 392 for the *TC*1 or *TC*2 curve, respectively). The overall RMSE value was then calculated as

$$\mathrm{RMSE}_{ov} = \sqrt{\frac{1}{n_{\mathrm{o}}}\sum_{j=1}^{n_{\mathrm{o}}}(\mathrm{RMSE}_j)^2} \tag{28}$$

where n_{o} is the number of model outputs (i.e., four).

It can be observed from Table 3 that the results obtained in the simulation of the two curves are comparable for p_1, p_2, and T_2 (RMSE lower than 1% in both cases), while the RMSE for M_0 is different for the two curves and the values are considerably high (4.0% for *TC*1 and 1.7% for *TC*2 curve). For this reason, the overall RMSE value for the *TC*1 curve (about 2%) is twice the overall RMSE value for the *TC*2 curve (about 1%).

Success Rate. In order to further validate the model, a comparison between predictions and measurements for both curves was performed by calculating the success rate for each output. The success rate was determined as the ratio between the number of predicted values lying within measurement uncertainty (i.e., which do not deviate from the corresponding measured values more than the absolute measurement uncertainty) and the total number of predicted values (i.e., 1383 or 392 for *TC*1 or *TC*2 curve, respectively). The estimation of the absolute uncertainties for the measured quantities (reported in Table 4) was performed by using the results of the uncertainty analysis conducted in [18] for a single working point (N_{C} equal to about 29,000 rpm) of the compressor under investigation.

The results are reported in Table 4 for the four outputs (p_1, p_2, M_1, and T_2), by taking into consideration only measured and predicted values after 1 s from the beginning of the maneuvers, as outlined above. The results seem to be very encouraging for both curves since:

- Compressor inlet and outlet pressures are reproduced almost perfectly (success rate equal to 86% in the worst case);
- The success rate for the mass flow rate is not very high (especially for the *TC*1 curve), according to high RMSE values reported in Table 3;
- If T_2 measurement uncertainty as reported in [18] is considered (the *K*-type thermocouple used was on purpose calibrated in a thermostatic bath), the success rate is rather low (46% or 30% for the two curves). On the other hand, if the uncertainty associated to the standard type of this thermo-

Table 4 Ratio between the number of predicted values lying within measurement uncertainty and total number of predicted values (success rate)

Quantity	Uncertainty		Ref.	Success rate [%] *TC*1	Success rate [%] *TC*2
p_1	0.636	kPa	[18]	100	100
p_2	1.817	kPa	[18]	98	86
M_0	0.012	kg/s	[18]	50	90
T_2	1.0	°C	[18]	46	30
T_2	2.2	°C	[19]	84	62

couple (which is a Class 2 tolerance thermocouple [19], uncertainty equal to 2.2 °C) is considered, the success rate is more than acceptable (84% or 62%).

The results presented in this section in terms of success rate were obtained by comparing the difference between predictions and measured values to measurement uncertainty alone. Such a criterion is the most restrictive way to validate a code. In fact, as reported in [20] for computational fluid dynamics (CFD) code validation, a model can be considered validated if the difference between the measured and the computed values is lower than the combined uncertainty, which takes into account the combined uncertainty both in the measured value and in the predictions. In particular, the combined uncertainty for measured values (experimental data) takes into account experimental uncertainty. For the combined uncertainty in the predicted values, Coleman and Stern [20] propose to also consider the influence (1) of the numerical solution uncertainty and (2) of the simulation modeling uncertainty arising (a) from the use of previous experimental data and (b) from modeling assumptions. Thus, if all these effects were considered for success rate calculation, the success rate for the developed model would be undoubtedly higher. In any case, the comparison with the results of a similar analysis presented in [5] shows that the model can be considered clearly validated.

Conclusions

In the paper, a mathematical model for compressors dynamic simulation was developed and implemented through the MATLAB® SIMULINK® tool.

The physics-based approach allowed the determination of model parameter influence through a sensitivity analysis. The analysis showed that (i) intake duct friction factor mainly affects inlet compressor pressure and mass flow rate, (ii) exhaust duct friction factor influences outlet compressor pressure significantly, and (iii) an increase in the exhaust duct hydraulic mean diameter allows a greater mass flow rate, while outlet compressor pressure and outlet compressor temperature decrease.

The model was then successfully calibrated on a multi-stage axial-centrifugal small size compressor. Model validation against experimental data showed, for both considered test cases, that (i) predicted values closely follow experimental data, without appreciable delay between model and system response and (ii) for all model outputs, the number of predicted values which do not deviate from the corresponding measured values more than the absolute measurement uncertainty is clearly acceptable.

Future developments of the present study will deal with the implementation of the model which uses as an input the measured value of the torque supplied to the compressor instead of compressor rotational speed. Furthermore, neural networks will be set up in order to support already-developed physics-based models and to verify the capability of such a tool in dealing with transient data. Finally, compressor behavior in the presence of implanted faults and/or in off-design conditions will be investigated by means of both simulation tools (physics-based models and neural networks) in order to build a database in which malfunctions (ranked in type and severity) will be related to measured values and health indices variations.

Acknowledgment

The work was carried out with the support of the M.U.R.S.T. (Italian Ministry of University and Scientific & Technological Research). The author gratefully acknowledges Professor Roberto Bettocchi, Professor Pier Ruggero Spina, and Michele Pinelli PhD for the suggestions provided during the work and Dr. Mirko Morini for his precious support in the model setup.

Nomenclature

A = control volume frontal area
C = $c\rho V$ thermal capacity
c = specific heat
D_h = hydraulic mean diameter
e = specific energy
f = force per unit volume
J = moment of inertia
k = thermal conductivity, ratio of specific heats c_p/c_v
L = length
l = work per unit volume
M = mass flow rate
N = rotational speed
n_o = number of outputs
n_{pred} = number of predicted values
P = power
p = pressure
Q = quantity
q = heat per unit volume
R = radius, gas constant
r = radial coordinate, N_C/N_E gearbox velocity ratio
RH = relative humidity
RMSE = root mean square error
T = temperature
t = time
Tq = torque
u = specific internal energy
V = volume
v = flow velocity
x = axial coordinate
α = heat transfer coefficient, throttle valve position
β = pressure ratio
Γ = concentration
η = efficiency
λ = friction factor
ψ = flux
μ = $M\sqrt{T}/p$ corrected mass flow rate
ν = $N/\sqrt{T}$ corrected rotational speed
ρ = density

Subscripts and Superscripts

0,1,2,3 = model sections
amb = ambient
b = box
bf = body field
C = compressor
cool = cooling
E = electric motor
e = entering, external
fr = friction
g = generated
i = internal
l = leaving
meas = measured
o = outlet
oil = lube oil
op = orifice plate
ov = overall
p = potential, constant pressure
pred = predicted
r = resisting
ref = reference
s = shaft, supplied
stat = stationary
v = constant volume
w = wall
∞ = outside

References

[1] Madej, J., Longtin, K., and Smith, D.-P., 1996, "Monitoring and Diagnostics Service Delivery System," *Proc., 39th GE Turbine State-of-the-Art Technology Seminar*, GE Ed., GER-3956, Schnectady, Aug. 26–29, pp. 1–8.

[2] Bettocchi, R., and Spina, P. R., 1999, "Diagnosis of Gas Turbine Operating Conditions by Means of the Inverse Cycle Calculation," ASME Paper No. 99-GT-185.

[3] Tsalavoutas, A., Aretakis, N., Mathioudakis, K., and Stamatis, A., 2000, "Combining Advanced Data Analysis Methods for the Constitution of an Integrated Gas Turbine Condition Monitoring and Diagnostic System," ASME Paper No. 2000-GT-0034.

[4] Bettocchi, R., Pinelli, M., Spina, P. R., Venturini, M., and Sebastanelli, S., 2001, "A System for Health State Determination of Natural Gas Compression Gas Turbines," ASME Paper No. 2001-GT-0223.

[5] Blotemberg, W., 1993, "A Model for the Dynamic Simulation of a Two-Shaft Industrial Gas Turbine With Dry Low No_x Combustor," ASME Paper No. 93-GT-355.

[6] Schobeiri, M. T., Attia, M., and Lippe, C., 1994, "GETRAN: A Generic, Modularly Structured Computer Code for Simulation of Dynamic Behavior of Aero- and Power Generation Gas Turbine Engines," ASME J. Eng. Gas Turbines Power, **116**, pp. 483–494.

[7] Bettocchi, R., Spina, P. R., and Fabbri, F., 1996, "Dynamic Modeling of Single-Shaft Industrial Gas Turbine," ASME Paper No. 96-GT-332.

[8] Bianchi, M., Peretto, A., and Spina, P. R., 1998, "Modular Dynamic Model of Multi-Shaft Gas Turbine and Validation Test," *Proc. "The Winter Annual Meeting of ASME,"* AES - 38, ASME, New York, pp. 73–81.

[9] De Mello, F. P., and Ahner, D. J., 1994, "Dynamic Models for Combined Cycle Plants in Power System Studies," IEEE Trans. Power Appar. Syst., **9**(3), 7698–7708.

[10] Camporeale, S. M., Fortunato, B., and Mastrovito, M., 2002, "A High-Fidelity Real-Time Simulation Code of Gas Turbine Dynamics for Control Applications," ASME Paper No. GT-2002-30039.

[11] Botros, K. K., Jungowski W. M., and Richards D. J., 1996, "Compressor Station Recycle System Dynamics During Emergency Shutdown," ASME J. Eng. Gas Turbines Power, **118**, pp. 641–653.

[12] Baojie, L., Hongwei, W., Huoxing, L. Hongjun, Y., Haokang, J., and Maozhang, C., 2003, "Experimental Investigation of Unsteady Flow Field in the Tip Rregion of an Axial Compressor Rotor Passage at Near Stall Condition With SPIV," ASME Ppaper No. GT2003-38185.

[13] Sanders, A. J., Hassan, K. K., and Rabe, D. C., 2003, "Experimental and Numerical Study of Stall Flutter in a Transonic Low-Aspect Ratio Fan Blisk," ASME Paper No. GT2003-38353.

[14] Cellai, A., Ferrara, G., Ferrari, L., Mengoni, C. P., and Baldassarre, L., 2003, "Experimental Investigation and Characterization of the Rotating Stall in a High Pressure Centrifugal Compressor. Part IV: Impeller Influence on Diffuser Stability," ASME Paper No. GT2003-38394.

[15] Dedoussis, V., Mathioudakis, K., and Papailiou, K. D., 1997, "Numerical Simulation of Blade Fault Signatures From Unsteady Wall Pressure Signals," ASME J. Eng. Gas Turbines Power, **119**, pp. 362–369.

[16] Aretakis, N., Mathioudakis, K., and Stamatis, A., 1998, "Blade Fault Recognition Based on Signal Processing and Adaptive Fluid Dynamic Modeling," ASME J. Eng. Gas Turbines Power, **120**, pp. 543–549.

[17] Changduk, K., Hongsuk, R., and Kangtaek, L., 2003, "Steady-State and Transient Simulation of Turboprop Engine Using Simulink Model," ASME Paper No. GT2003-38181.

[18] Bettocchi, R., Pinelli, M., and Spina, P. R., 2003, "A Multi-Stage Compressor Test Facility: Uncertainty Analysis and Preliminary Test Results," ASME J. Eng. Gas Turbines Power, **127**(1), 170–177.

[19] *Annual Book of ASTM Standards, Temperature Measurement*, 1998, 14.03, American Society for Testing and Philadelphia, PA.

[20] Coleman, H. W., and Stern, F., 1997, "Uncertainties and CFD Code Validation," ASME J. Fluids Eng., **119**, pp. 795–803.

Journal of Turbomachinery

Erratum

Erratum: "Development and Experimental Validation of a Compressor Dynamic Model" [Journal of Turbomachinery, 2005, 127(3), pp. 599–608]

M. Venturini

The error is very severe and, in my opinion, negatively affects the quality of the whole paper, since it causes a misunderstanding of the technical content presented.

Thus, the following sentence on p. 604, second column, line 14 of the printed version:

… both taken at quasi-imaginary spin orbit (ISO) conditions …

should be changed into:

… both taken at quasi-ISO conditions …

In fact, the acronym ISO stands for "International Organization for Standardization", and not for "imaginary spin orbit". Since the acronym ISO is a standard for machine performance evaluation and is well known in the field of turbomachines and of energy systems, I suggest to only maintain the acronym ISO.

